



**HAL**  
open science

## Seismic design of a low-carbon building constructed with in-situ produced compressed earth blocks

Noura Zarzour, Maria Paola Santisi D'avila, E. Diego Mercerat, Luca Lenti,  
Michel Oggero

► **To cite this version:**

Noura Zarzour, Maria Paola Santisi D'avila, E. Diego Mercerat, Luca Lenti, Michel Oggero. Seismic design of a low-carbon building constructed with in-situ produced compressed earth blocks. *Soil Dynamics and Earthquake Engineering*, 2024, 187, pp.108990. 10.1016/j.soildyn.2024.108990. hal-04717979

**HAL Id: hal-04717979**

**<https://hal.science/hal-04717979v1>**

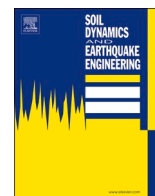
Submitted on 3 Oct 2024

**HAL** is a multi-disciplinary open access archive for the deposit and dissemination of scientific research documents, whether they are published or not. The documents may come from teaching and research institutions in France or abroad, or from public or private research centers.

L'archive ouverte pluridisciplinaire **HAL**, est destinée au dépôt et à la diffusion de documents scientifiques de niveau recherche, publiés ou non, émanant des établissements d'enseignement et de recherche français ou étrangers, des laboratoires publics ou privés.



Distributed under a Creative Commons Attribution 4.0 International License



## Seismic design of a low-carbon building constructed with in-situ produced compressed earth blocks

Noura Zarzour<sup>a,c</sup>, Maria Paola Santisi d'Avila<sup>a,\*</sup>, E. Diego Mercerat<sup>b</sup>, Luca Lenti<sup>b</sup>, Michel Oggero<sup>c</sup>

<sup>a</sup> Université Côte D'Azur, Polytech'Lab, UPR 7498, Biot, France

<sup>b</sup> CEREMA, Repsody, Sophia Antipolis, France

<sup>c</sup> FILLATER, Nice, France

### ARTICLE INFO

#### Keywords:

Geo-sourced construction material  
Compressed earth block  
Masonry building  
Equivalent frame approach  
Ductility  
Behavior factor  
Pushover analysis

### ABSTRACT

The seismic design of buildings erected using new low-carbon construction materials needs the development of a reliable methodology. In this research, a pilot project of a compressed earth block (CEB) masonry building in a medium-high seismic hazard zone in Southern France is developed. The CEBs are produced in-situ, using a machine, and are used as construction material for low-rise masonry buildings. This innovative low-carbon construction technology permits the reuse of local soil, removed during earthworks, with consequent reduction of energy consumption related to its collection, transport, recovery, and disposal. Even if the CEB masonry building is a promising low-carbon construction, its structural performance assessment, especially in seismic zones, is a challenging issue.

Starting from the experimental characterization of material mechanical parameters, the seismic design approach focuses on the modal characteristics of the structure, the expected building ductility, and seismic performance assessment in terms of both displacement and force. The behavior factor for a CEB masonry building is an original result of this research. The equivalent frame model adopted for structural design of load-bearing masonry is validated, after the building construction, by comparing the dynamic properties obtained by both numerical and operational modal analysis. Moreover, the modal analysis highlights the impact of the timber slab stiffness on the dynamic response of masonry buildings and suggests that a careful timber slab conception improves the structural behavior under seismic loading.

### 1. Introduction

Intending to achieve low-carbon building construction and sustainable development, there is a growing interest in the use of local materials fabricated from natural resources extracted at (or near) the construction site. The reuse of geo-sourced materials for building construction [1] derives from ancient techniques (rammed earth, fired and unfired earth bricks). In particular, compressed earth blocks (CEBs) are a promising construction material potentially contributing to a more sustainable building industry [2]. According to Valenzuela et al. [3], the CEB production process is outlined by three stages: raw material characterization, preparation and manufacturing, and block testing. The physical and mechanical properties of raw materials and blocks are performed according to standardized experimental tests. The optimization of CEB strength and carbon balance involves the choice of a

stabilizer and its percentage, the water content, and compaction pressure [4–7].

In the framework of this research, an advancement in geo-construction is obtained using press machines installed in (or near) the construction site to produce the CEBs, using the soil removed during the leveling of the construction site. The reuse of local soil removed during earthworks, as construction material, reduces gas emissions and energy consumption related to collection, transport, recovery, and disposal. Even though in-situ produced CEB masonry is a low-carbon construction technology, the assessment of structural performance, especially in medium to high seismic hazard zones, poses significant challenges that could limit their use. First, as the soil physical properties and water content change for each construction site, the compression force and the stabilization are deduced as a function of the performance target in terms of compression strength expected for the CEB, as well as

\* Corresponding author. Université Côte d'Azur, Polytech'Lab, UPR 7498, 930, Route des Colles, 06410, Biot, France.

E-mail address: [msantisi@unice.fr](mailto:msantisi@unice.fr) (M.P. Santisi d'Avila).

of carbon balance. On the other hand, the use of earth masonry as construction material remains limited by the difficulty of correctly evaluating the performance of the load-bearing structure under dynamic action, which can be prohibitive for questions of technical certification and insurability of a new construction in seismic zones. For example, the force reduction factor  $q_0$  [8], is a key parameter to be estimated for the analysis of the structural response of CEB masonry buildings under seismic loading, according to design codes [9,10]. It is defined as the ratio between the maximum base shear force from elastic and elasto-plastic analysis and represents the structure capacity to dissipate hysteretic energy. A causal relationship exists between the force reduction factor and the structure displacement ductility [11,12], conceptually defined as the ultimate to yield displacement ratio. The force reduction factor is well-known for classic construction materials but must be estimated for new geo-sourced materials.

The equivalent frame (EF) approach [13–16] is a modeling technique accepted in the current version of Eurocode 8 [9] for earthquake design of load-bearing masonry buildings. It strikes a balance between result accuracy and computational efficiency in engineering practice. In the EF model, it is assumed a global box-like behavior of the building and that out-of-plane failure modes of walls are prevented. The building structure is composed of deformable wall elements, such as piers and spandrels, interconnected by rigid nodes. In fact, the observation of damage after seismic events and experimental campaigns highlights zones between the resisting elements without significant signs of damage. In this research, the building model is obtained using the EF approach developed by Lagomarsino et al. [15]. Piers and spandrels are modeled using an equivalent beam element having elastic-perfectly plastic (EPP) behavior [17]. The interaction between shear, bending, and axial force, in the beam response, is considered according to the definition of strength domains [15,18–20]. The latter are calibrated using the strength parameters obtained by compression and shear tests on masonry triplets. The intersection of the strength domains (bending moment and shear versus axial force curves) gives information about the expected in-plane failure mode of the masonry panel (bending-rocking or shear mechanisms).

The dynamic properties and ductility of masonry buildings are not only associated with the material mechanical parameters and masonry wall behavior, but they are strongly influenced by the box-like behavior of the building, due to the chaining of walls and effective connection between each slab and walls. In particular, the slab rigidity and its connection with walls directly affect the dynamic properties and ductility [21–23]. In particular, Pavanetto et al. [22] identify the in-plane shear modulus of timber slabs as a key parameter to characterize the slab stiffness and its impact on the building behavior. According to Salvalaggio et al. [21] and Zarzour et al. [23], an increased in-plane shear modulus of timber slabs leads to global mode shapes with effective masses concentrated in the first mode shapes, inducing a better dynamic behavior of the masonry structure.

This research proposes a seismic design methodology integrating the use of a novel construction material adopted for masonry buildings. In particular, it is applied for a pilot project of a CEB masonry building. The building was constructed in 2023 in Southern France, in the historical center of Charleval (43° 43'09.1" N, 5° 14'36.7" E) that is a medium-high seismic hazard zone, identified as 4 in the French seismic hazard zonation map [24]. The intended use of the building is a health center and the level of importance is II, according to the Eurocode 8 [9].

The design methodology includes the selected approach for characterizing the mechanical parameters of geo-sourced materials, estimating the structure displacement ductility capacity and demand, and assessing the building stability for the combination of dead, live, and seismic load. The methodology of validation for the three-dimensional (3D) EF model of the building involves the comparison of dynamic features obtained by numerical and operational modal analysis [25–27]. In fact, after the building construction, the structural response to under ambient vibration is recorded during a measurement campaign using velocity sensors.

The dynamic features of the building, in terms of natural frequencies and mode shapes, are obtained by inversion of the recorded structural response to ambient vibrations using operational modal analysis tools [28,29].

After validation of the EF model, the building displacement capacity is recalculated using the calibrated model and performing a pushover analysis [30]. Then, the building stability is assessed [31] by comparing the displacement capacity and demand. The displacement demand is obtained according to the N2 method [32] as proposed by Eurocode 8 [9]. In this research, the stability verification is undertaken also in terms of load capacity, using the force reduction factor  $q_0$ , as proposed by Zarzour et al. [33].

In the pilot project of the CEB masonry building, timber slabs with timber joists and planks are adopted, as in traditional masonry buildings, for structural and environmental performance. After the analysis of the mode shapes for the CEB masonry building, the impact of a stiffer timber slab is investigated to correct the effects of plan irregularity in the structure.

## 2. Pilot project of a CEB masonry building

The CEB production technology, using the local soil in the construction site, is adopted to build a 3-story masonry building, whose intended use is a health center. The building has importance class II and the ground type is classified as B, according to the European categorization [9] characterized by a flat topography. It is located in the city center of Charleval (43° 43'09.1" N, 5° 14'36.7" E) in Southern France, in a medium-high seismic hazard zone, identified as 4 in the French seismic hazard map [24].

### 2.1. Geo-sourced construction materials

The geo-sourced construction materials adopted in the analyzed pilot project are CEB and non-reinforced plum concrete (PC) in which medium and large-sized stones are used as aggregate. The CEBs are fabricated in-situ using the soil removed after leveling and other earthworks (Fig. 1a). The fine-grained soil is mixed with water. The mixing quantities during the fabrication process are influenced by the soil composition and water content. Depending on the soil granulometry, coarse grains can be added to improve the final strength. Moreover, the soil is cement-stabilized using a quantity of hydraulic binder lower than 8 % of the soil dry weight to attain a suitable compressive strength. The use of a press machine (Fig. 1b) allows on one side the achievement of a fixed block dimension and a target compressive strength and on the other side the industrialization of the CEB production process. The machine is placed close to the construction site, where the extracted resources are stored, strongly reducing the energy consumption and carbon dioxide emissions related to the soil removal after earthworks and transportation of construction materials.

The CEB masonry buildings can be constructed only if fine-grained soil is available at the construction site, characterized by plasticity properties. It is possible to produce CEB if the soil contains between 10 and 35 % of clay, with clay activity classified as medium ( $A_{CB} < 13$ ). The clay activity  $A_{CB}$  is the methylene blue value [34] divided by the particle content passing through a 2  $\mu\text{m}$  sieve [35]. Soil classification is determined through granulometric analysis and a methylene blue test to evaluate its clay activity, following the French standard [36]. The average clay content in the used soil is 12.6 %.

Fine-grained soil at the surface of the construction site is used to fabricate CEBs. Nevertheless, the lack of a sufficient quantity of fine-grained soil justifies the use of PC for cross-walls. A gravelly soil for PC is present in deeper layers, but to avoid deeper excavations it is taken from a close quarry. The granulometry and physical properties of soil used to produce the CEB and PC in this pilot project are listed in Tables 1 and 2. In CEB, the maximum diameter of soil is restricted to 20 mm to ensure the material homogeneity and guarantee a good aspect of the

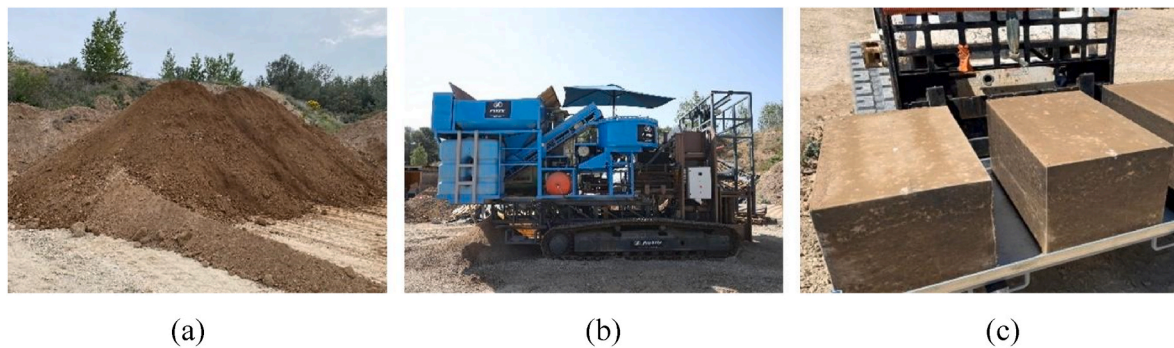


**Fig. 1.** In-situ produced compressed earth blocks for the pilot project of masonry building in Southern France: (a) earth removed during the leveling of the construction site; (b) press machine used to produce compressed earth blocks; (c) 80 × 40 × 50 cm compressed earth blocks.

**Table 1**  
Sieve analysis and classification of soil.

Geo-sourced material	Soil type	D <sub>max</sub> (mm)	Percent passing					GTR
			50 mm (%)	2 mm (%)	80 μm (%)	63 μm (%)	2 μm (%)	
CEB	Sand with silt	33	100	84.0	46.4	46.0	9.7	A1
PC	Gravel with sand	45	100	52.9	14.2	12.8	2.2	B5

D<sub>max</sub>: maximum diameter; GTR: French GTR soil classification [36].

**Table 2**  
Soil properties.

Geo-sourced material	Soil type	ρ (kg/m <sup>3</sup> )	w (%)	PL (%)	LL (%)	PI	MBV
CEB	Sand with silt	2648	12.8	20	24	4	1.14
PC	Gravel with sand	2628	4.4	–	–	–	0.23

ρ: mass density; w: water content; PL: plastic limit; LL: liquid limit; PI: plasticity index; MBV: methylene blue value.

block. In PC, the maximum diameter of stone aggregate is 300 mm. A Portland-limestone cement classified as CEM II/B-LL 32.5R according to the European standard [37] is adopted.

The in-situ produced CEB (Fig. 2a) is 80 cm long, 40 cm high, and

50 cm thick. The CEBs undergo 28-day curing before their use on the construction site, including 14 days of wet curing under cover immediately after fabrication and 14 days of drying protected from the weather. This curing allows the hydraulic uptake of the stabilizing binder and the gradual evaporation of excess water.

The PC (Fig. 2b) is produced in-situ by mixing the stones with sand and cement, using a mixer. A different cement dosage is used for cross-walls (190 kg/m<sup>3</sup>) and for the beams where tie rods are incorporated (355 kg/m<sup>3</sup>), expressing the cement dosage as the mass of cement per cubic meter of concrete. According to European standard [38] the water dosage is carefully calibrated to maintain a water-to-cement mass ratio lower than 0.6 for beams and 1 for cross-walls.

CEBs are cut with a water-blade saw to obtain the specimens for laboratory tests. The mechanical parameters of CEB and PC are obtained by the following standardized experimental tests: twelve compression tests are performed according to the European standard [39] on 20 × 20 × 40 cm CEB specimens and five compression tests are carried out

**Table 3**  
Mechanical parameters of the compressed earth blocks (CEB) and plum concrete (PC) determined from laboratory tests.

		CEB	PC
Mass density	ρ (kg/m <sup>3</sup> )	1990	2100
Elastic modulus	E (MPa)	1230	14800
Average compressive strength	$\bar{f}$ (MPa)	6.0	8.0
Pure shear strength	f <sub>vo</sub> (MPa)	0.1	–
Friction coefficient	tan φ	0.9	–
Average tensile strength	f <sub>t</sub> (MPa)	–	0.95

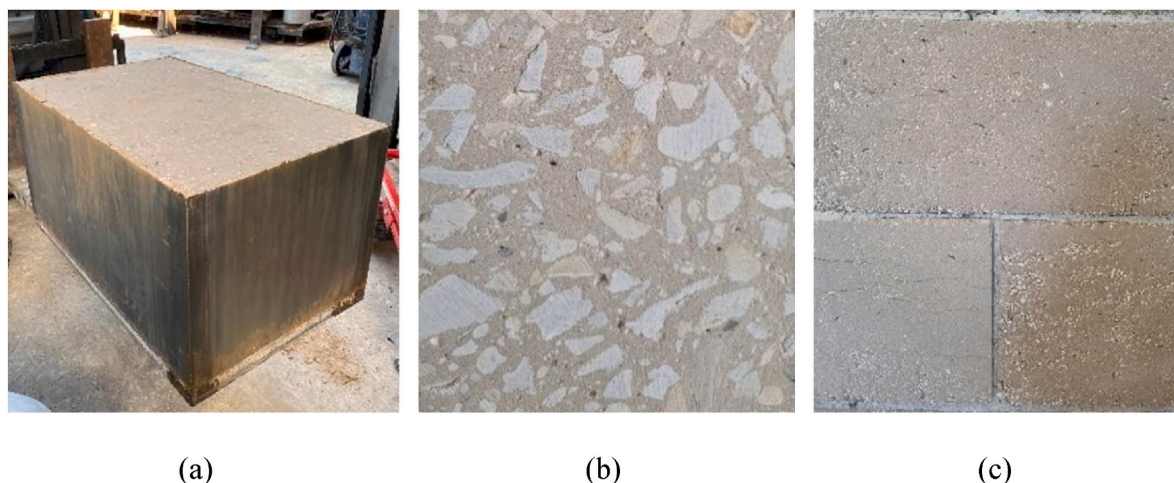


**Fig. 2.** (a) 80 × 40 × 50 cm compressed earth block; (b) plum concrete; (c) compressed earth block masonry walls.



[40] on  $16 \times 32$  cm cylindrical PC samples, to obtain the compressive strength  $\bar{f}$  and the elastic modulus  $E$  (Table 3). Moreover, six splitting tensile tests [41] are performed on cylindrical PC samples to estimate the average tensile strength  $f_t$  (Table 3). The ready-to-use mortar selected for the CEB masonry walls has average compressive strength  $f_{mo} = 6.5$  MPa. Nine standardized shear tests on the block-mortar interface (NF EN 1052-3/A1) are realized and also ten non-standardized shear tests on  $45^\circ$  inclined couplets are carried out; the shear strength in pure shear  $f_{v0}$  and friction coefficient  $\tan \varphi$  are deduced by linear regression of all the results (Table 3). Both horizontal and vertical joints in the CEB masonry walls are 10 mm thick (Fig. 2c).

The mechanical parameters of masonry, defined as a homogenized material, are necessary for the building model calibration. In this research, considering the regularity of CEB masonry (Fig. 2c), the mechanical parameters of masonry (Table 4) are obtained according to the Eurocode 6 [42]. The compressive strength of masonry is estimated using the homogenization formula  $f_m = 0.45 f_b^{0.7} f_{mo}^{0.3}$ , where the adopted normalized strength of CEB is  $f_b = 1.25 \bar{f} = 7.5$  MPa and  $f_{mo} = 6.5$  MPa, the masonry elastic modulus in compression is  $E = 1000 f_m$  and the shear modulus is  $G = 0.4 E$ . The pure shear strength for the PC is adopted equal to the tensile strength obtained by the splitting test. According to Eurocode 6 [42], the friction coefficient  $\tan \varphi = 0.4$  is assumed for both materials and the tensile strength in shear is limited to  $f_{v,lim} = 0.065 f_b$  for CEB and  $f_{v,lim} = 0.065 \bar{f}$  for PC.

## 2.2. Building structure

In this pilot project of a 3-story CEB masonry building (Fig. 3a) in a seismic zone, CEBs are used for the façades (Fig. 3b and c) and PC is used for the foundation, basement walls, cross-walls (Fig. 3d), and beams where tie rods are incorporated. The connection between CEB walls is achieved through wall interlocking (Fig. 3c). Moreover, timber joists and planks are adopted for slabs and the roof. The vertical and horizontal sections of the pilot building are shown in Figs. 4 and 5, respectively. All CEB masonry and PC walls in Fig. 5 are bearing walls carrying both vertical and horizontal loads. The wall of the façade is 50 cm thick (see Fig. 5) to improve the building response to horizontal loads. The non-reinforced PC cross-walls are 38 cm or 40 cm thick. The connection between PC and CEB walls is realized using vertical tie rods placed at the extremity of PC walls and anchored hooks embedded in the horizontal mortar joints, whose spacing is equal to the height of CEB. The reservation in the PC wall is then cast.

Timber slabs with timber joists and planks are adopted, as in traditional masonry buildings. Such flexible slab is preferred according to the observations of Binda et al. [43], showing that the use of stiffer reinforced slabs, such as rib-and-block concrete slabs with tie beams inserted into the wall thickness, does not represent a more efficient solution because they do not prevent the out-of-plane collapse of the masonry.

In the construction plans in Fig. 5, the direction of timber joists is indicated using two different symbols to distinguish the (hidden) OSB slab in Fig. 6a and the (visible) interlocked board slab in Fig. 6b. The one-way timber slab in Fig. 6a is composed of timber joists and oriented strand board (OSB) plank and it is hidden from the view of users. The

**Table 4**

Mechanical parameters of the CEB masonry and plum concrete (PC) used in the equivalent frame model of the building.

		CEB masonry	PC
Mass density	$\rho$ (kg/m <sup>3</sup> )	1990	2100
Elastic modulus	$E$ (MPa)	3230	14800
Shear modulus	$G$ (MPa)	1292	5920
Average compressive strength	$f_m$ (MPa)	3.23	8.0
Pure shear strength	$f_{v0}$ (MPa)	0.1	0.95
Friction coefficient	$\tan \varphi$	0.4	0.4
Tensile strength in shear	$f_{v,lim}$ (MPa)	0.5	0.5

visible slab in Fig. 6b consists of joists and good-looking interlocked thin boards before the superposition of an uncoupled OSB. GL24h is the strength class [44] of wood used for the joists and interlocked boards. The mechanical parameters of wood and OSB [45] used to estimate the mechanical parameters of slabs are given in Table 5.

The timber slabs are connected to the PC cross-walls, incorporating steel anchors (Fig. 6c), through the casting of a PC beam. A horizontal tie rod (Fig. 6c) is also embedded in these PC beams, at the slab level, to connect the PC cross-wall to the façade, preventing out-of-plane failures and ensuring a global box-like behavior of the building during seismic loading.

## 2.3. 3D equivalent frame model of the CEB masonry building

The EF model of the masonry building, presented in Fig. 7, is developed using the 3Muri software by S.T.A. DATA (Release 13.9.0.1). The model assumes a rigid connection between walls and between slab and wall, presuming a global box-like behavior. The hypothesis of prevented out-of-plane wall failure is guaranteed by the high thickness of CEB [46,47] which is equal to 50 cm. In the framework of the EF approach, the in-plane behavior of piers and spandrels is modeled using a nonlinear beam element [15] with an EPP behavior. The plateau in the bilinear response of piers and spandrels is defined as the minimum strength obtained by the coupling of strength domains related to in-plane failure modes, such as bending-rocking, sliding shear, and block cracking in tension. The foundation is assumed as a fixed base. In the 3D numerical model, the arched openings in the longitudinal façade and cross-walls are assumed as rectangular openings limited by spandrels.

The timber roof is assumed as non-structural, whereas the slabs are modeled as structural components. The elastic modulus in compression in the main orthotropy direction of the slab is deduced as  $E_1 = (E_w A_j) / (i t_{eff}) + E_p$ , where  $i$  is the joist spacing,  $A_j$  is the joist cross-sectional area, and  $t_{eff}$  is the diaphragm effective thickness.  $E_w$  and  $E_p$  are the elastic moduli in compression of wood joists and plank, respectively. In the case of the OSB plank,  $E_p$  is assumed equal to the OSB elastic modulus  $E_{OSB}$  and the shear modulus of the slab  $G_{12}$  is assumed equal to the OSB shear modulus  $G_{OSB}$ . In the case of interlocked wood board plank,  $E_p$  is equal to the elastic modulus of wood. Whereas, the shear modulus  $G_{12}$  of the slab with interlocked thin boards is not well-known and it is obtained by calibration, as explained in Section 3. In the secondary orthotropy direction, the elastic modulus  $E_2$  is set to zero due to the absence of joists.

## 3. Validation of the CEB masonry building model

The methodology selected for the validation of the 3D equivalent frame model of the building involves the comparison of dynamic features of the building estimated by numerical and operational modal analysis. In fact, the inversion of the recorded structural response to ambient vibrations provides the building natural frequencies and mode shapes that are compared with those estimated by the direct (numerical) analysis. During the measurement campaign, six Guralp CMG40T velocity sensors are installed inside the building at each set-up. The velocity time histories are synchronized by connecting the six velocity sensors to a CityShark digitizer. The structure motion in terms of velocity time history is recorded for a duration of 30 min, using a sampling frequency of 200 Hz.

### 3.1. Natural frequencies and timber slab stiffness calibration

The Frequency Domain Decomposition technique [28,29] is the operational modal analysis tool adopted to identify the first natural frequencies and related mode shapes of the structure. All calculations are carried out using the MACity code [48]. The first six singular value spectra of the cross power spectral density matrix, displayed in Fig. 8a,

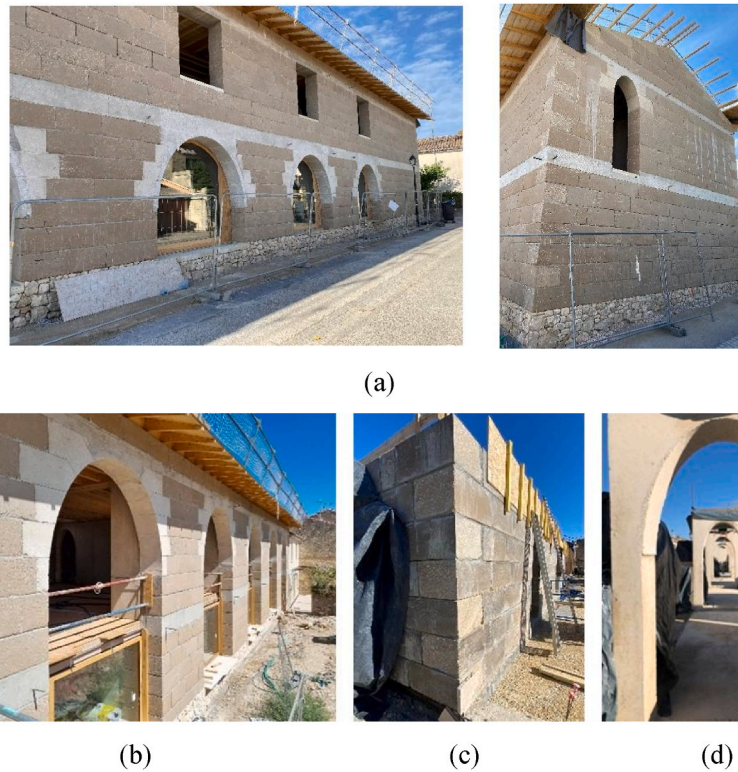


Fig. 3. Pictures of the pilot project: (a) 3-story compressed earth block (CEB) masonry building; (b) building façade composed of CEB masonry walls and plum concrete arcs (lighter color); (c) interlocking masonry walls; (d) non-reinforced plum concrete cross-walls.

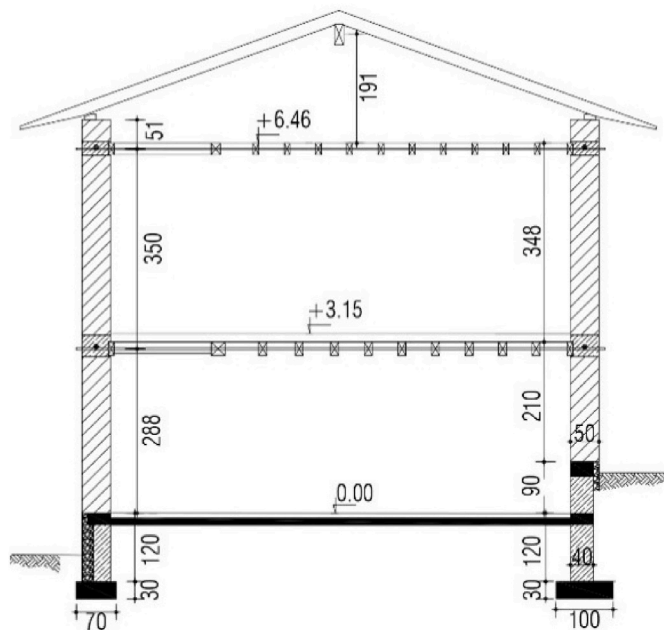


Fig. 4. Vertical section of the CEB masonry building.

are obtained using all the recorded signal components. The first natural frequencies, defined by peak picking from the first singular value spectrum, are  $f_1 = 10.1$  Hz,  $f_2 = 12.5$  Hz and  $f_4 = 14.3$  Hz. The third natural frequency  $f_3 = 12.8$  Hz, related to the longitudinal mode, is hidden in the singular value spectra in Fig. 8a. It is detected by peak picking from the singular value spectra obtained using only the longitudinal component of motion of each sensor (Fig. 8b). According to the random decrement technique (Cole 1973), low-strain structural

damping is estimated in the range [1.7 – 2.1 %] for the first four modes and then, a damping ratio  $\zeta = 2\%$  is adopted in the numerical model.

First, the geometry of the building (Fig. 7a) is reproduced according to construction plans and then, the dimensions are checked in-situ for the validation of the EF model. Since the building is unoccupied and without non-structural elements (partition walls, doors, lift, grids) during the measurement campaign, the uncertainty is not related to the live load that is assumed zero in the EF model. If the mechanical parameters in Table 4 are used for CEB masonry and PC and those in Table 5 for timber slabs, the building fundamental frequency matches with the result of operational modal analysis, but important discrepancies are obtained for the higher natural frequencies. In this first attempt, the shear modulus of interlocked board slabs (Fig. 6b) is assumed equal to the modulus of wood  $G_{12} = 720$  MPa.

If the elastic mechanical parameters of walls are modified, the match of fundamental frequency is lost. Since the first, second, and fourth modes are localized translations, the uncertainty does not seem related to the elastic moduli of the walls. The uncertainty is more related to the rigidity of diaphragms.

Finally, the key parameter permitting to match the first four natural frequencies (Table 6) and their corresponding mode shapes is the shear modulus  $G_{12}$  of slabs with interlocked thin boards (Fig. 6b). After the calibration of the timber slab stiffness, by setting  $G_{12} = 500$  MPa, negligible errors are obtained for the first four natural frequencies (Table 6). The rigidity of the visible slab is diminished by the discontinuity of interlocked thin boards (Fig. 6b). In conclusion, the mechanical parameters of CEB and PC walls, adopted in the building model, appear reliable.

### 3.2. Mode shapes

The first four mode shapes obtained through operational and numerical modal analysis (Fig. 9) are compared and the modal assurance criterion MAC [49] is calculated (Table 6).

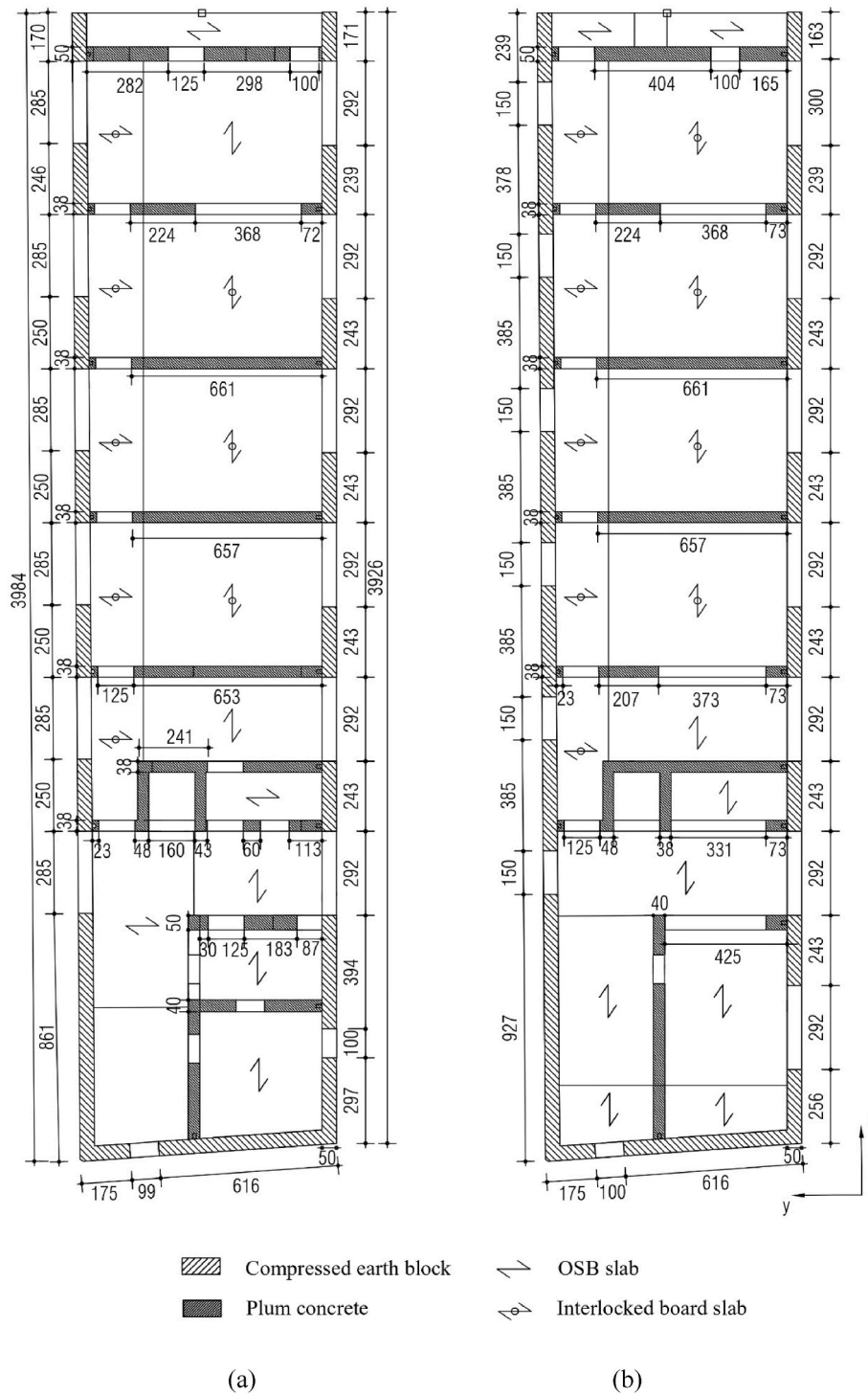


Fig. 5. Horizontal section of the first (a) and second (b) level of the CEB masonry building. The direction of the timber joists is indicated. All dimensions are in centimeters.

According to the results, the EF model is considered fully validated by the measurements. The first, second, and fourth mode shapes are characterized by a partial movement of the building in the transversal y-direction (according to the coordinate system in Fig. 5). This effect is a consequence of the high aspect ratio (almost four) and timber slab flexibility. The third one corresponds to a translational mode in the longitudinal x-direction. The gap in terms of natural frequency for the first translational mode shape in each direction (modes shapes 1 and 3) suggests a difference in terms of global inertia in the two orthogonal directions and a consequent plan irregularity. The high building aspect

ratio (almost four) and timber slab flexibility induce these three mode shapes (1, 2 and 4) with a partial movement of the building in transversal y-direction.

#### 4. Ductility estimation and stability verification

A pushover analysis [30] is performed using the 3D numerical model, in which a quasi-static horizontal load is incrementally applied until the building reaches the collapse. The uniform and modal load distributions are applied along the building height, according to



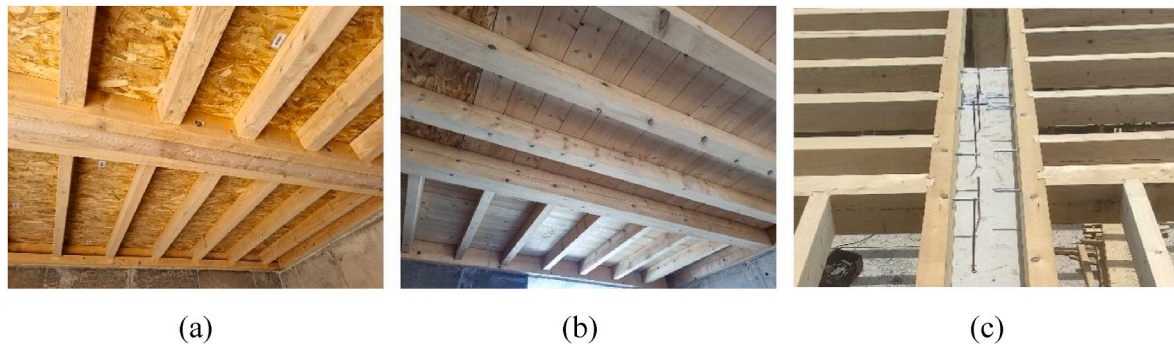


Fig. 6. Timber slabs: (a) oriented strand board (OSB) and joists; (b) good-looking interlocked thin boards and joists; (c) connection between a plum concrete wall and timber slabs before casting of the beam.

Table 5  
Mechanical parameters of wood and oriented strand board (OSB).

		Wood	OSB
Mass density	$\rho$ (kg/m <sup>3</sup> )	400	600
Elastic modulus	$E$ (MPa)	11600	3800
Shear modulus	$G$ (MPa)	720	1080
Compressive strength	$f_m$ (MPa)	34	15.9

Eurocode 8 [9]. The adopted multimodal distribution is proportional to the structure deformation in a linear elastic regime (obtained by combining the modes involving a cumulative effective mass not lower than 90 % of the building mass). The uniform distribution is proportional to the horizontal acceleration profile with height, assumed constant as in a plastic phase.

As discussed in Section 3.2, the first, second, and fourth mode shapes (Fig. 9) are characterized by a partial movement of the building in y-direction (coordinate system in Fig. 5). For this reason, the unimodal load distribution (proportional to the structure deformation of only one mode shape) is discarded for the pushover analysis.

The pushover curve of the 3D building represents the relation between the base shear force and the top floor displacement. In particular, the average top displacement weighted on nodal masses is considered [17]. The pushover analysis is carried out by imposing the horizontal load in the longitudinal and transversal direction of the building ( $\pm x, \pm y$ ) and an eventual accidental mass eccentricity in each direction ( $0, \pm 5\%$ ). Twelve analyses are performed for the two load distributions (24 analyses in total).

The ultimate top floor displacement  $U_u$  in the pushover curve is selected as the lower value between the displacement at which a 20 % strength decay occurs after the peak strength and the displacement at the failure of the first pier element. It is assumed that the pier failure is reached when the drift exceeds the threshold of 0.4 % in shear and 0.8 % in bending, as defined in the Eurocode 8 [31] for the severe damage limit state.

The force reduction factor  $q_0$  is calculated using the methodology proposed by Zarzour et al. [33]. Accordingly, the pushover curves ( $F, U$ ) associated with the 3D building model are converted into capacity curves ( $f, u$ ) related to an equivalent SDOF system, by dividing both quantities by the modal participation factor  $\Gamma$  [32]. This reduces the computational cost for the behavior factor estimation. The ductility capacity is estimated as the ultimate to yield displacement ratio  $\mu_0 = u_u/u_y$ , where the yield displacement is taken at the intersection between the linear elastic and the perfect plastic phases, after the bilinear idealization of the capacity curve [50]. On the other side, a relation ( $\mu, q_0$ ) between ductility demand and force reduction factor is numerically obtained, considering the dynamic properties (natural period and damping ratio) and hysteretic behavior of the equivalent SDOF system. The force reduction factor  $q_0$  is deduced from the ( $\mu, q_0$ ) curve

corresponding to the ductility capacity  $\mu_0$ . The interested reader can refer to Zarzour et al. [33] for more details.

The stability verification is performed by ensuring that the building capacity is higher than the seismic demand. First, the displacement demand  $U_t$  has to not exceed the ultimate displacement  $U_u$ , related to the near collapse limit state [31]. According to the N2 method [32], as proposed by the Eurocode 8 [9], the displacement demand  $U_t$  is determined as

$$\begin{aligned}
 & U_t = \Gamma u_e & T_0 \geq T_C \\
 & U_t = \Gamma u_e & T_0 < T_C \quad \text{and} \quad f_y/m \geq S_e(T_0) \\
 U_t = \Gamma u_e / q_u (1 + (q_u - 1) T_C / T_0) \geq u_e & T_0 < T_C \quad \text{and} \quad f_y/m < S_e(T_0)
 \end{aligned} \tag{1}$$

where

$$u_e = S_e(T_0) (T_0 / (2\pi))^2 \tag{2}$$

and

$$q_u = m_0 S_e(T_0) / f_y \tag{3}$$

$S_e(T_0)$  is the elastic acceleration response spectrum for an equivalent SDOF system having fundamental period  $T_0$  and mass  $m_0$ . The transitional period  $T_C$  is the corner period between the constant acceleration and constant velocity part of the response spectrum. The load ratio  $q_u$  is defined as the target load for an equivalent SDOF system having unlimited elastic behavior, normalized with respect to the yield force  $f_y$  of the equivalent SDOF system which represents the plateau in the EPP capacity curve.

The verification in terms of displacement is strongly dependent on the accuracy of the numerical procedure to determine the ultimate displacement  $U_u$ . For this reason, the stability verification is performed also in terms of base shear force. The Italian code [51] imposes a limit of 4 for the load ratio  $q_u$  at the near collapse limit state. Moreover, according to Ref. [33], the load ratio  $q_u$ , related to the base shear force demand, has to not exceed the force reduction factor  $q_0$  of the building, associated with the building strength capacity and obtained from its relation with the building ductility capacity  $\mu_0$ .

#### 4.1. Pushover analysis

After the validation of the EF model, additional non-structural dead loads have been considered for the stability verification of the building: 210 kg/m<sup>2</sup> for the first floor, 51 kg/m<sup>2</sup> for the second floor, and 42 kg/m<sup>2</sup> for the timber roof. Moreover, the live load is fixed according to the European standard [52]: 250 kg/m<sup>2</sup> for the first floor, 50 kg/m<sup>2</sup> for the second floor and 50 kg/m<sup>2</sup> for the roof. Dead and live loads are combined with the horizontal seismic load according to the Eurocode 8



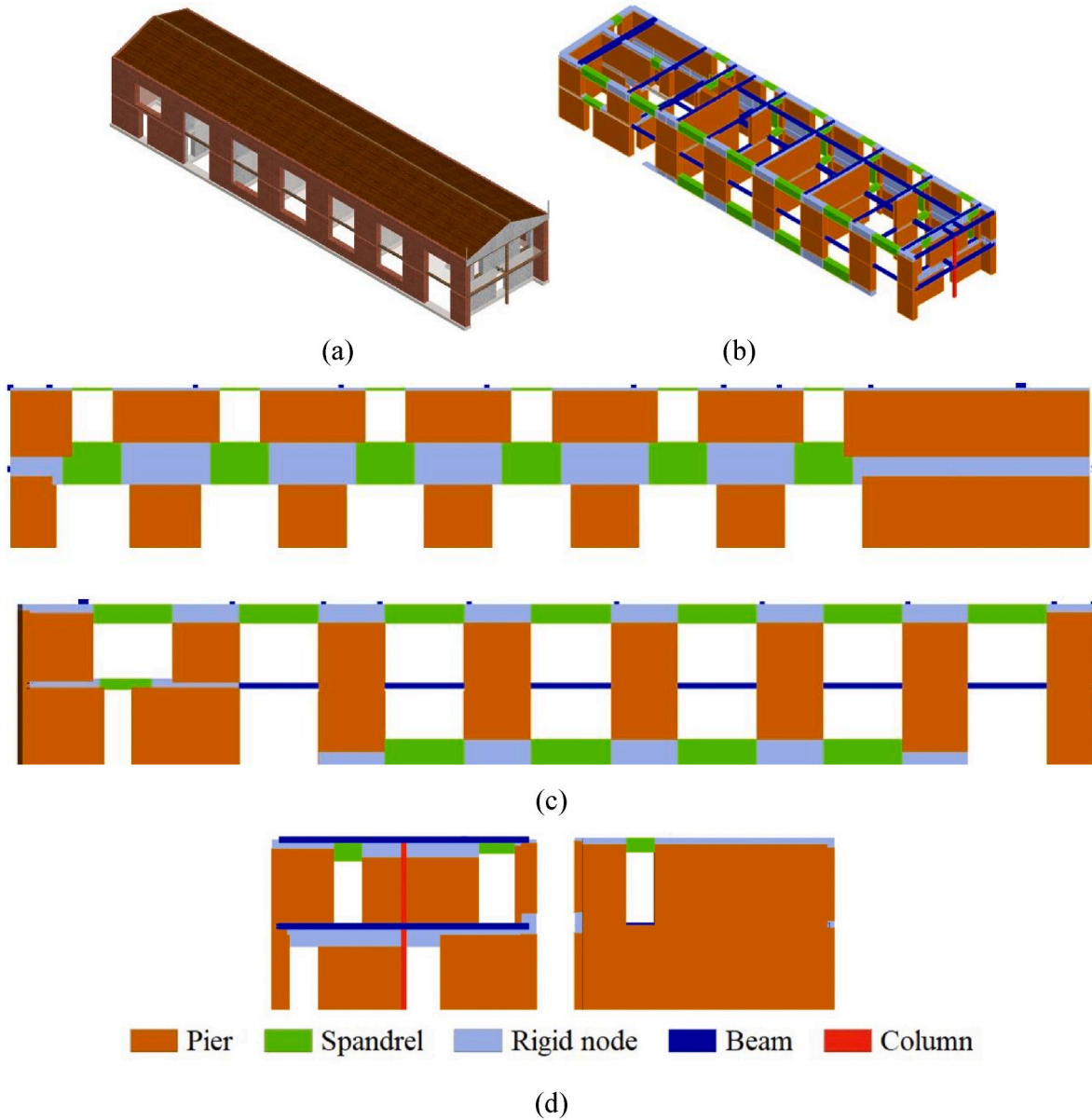


Fig. 7. Numerical model of the masonry building: (a) geometry; (b) 3D equivalent frame model; façades in (c) longitudinal direction and (d) transversal direction.

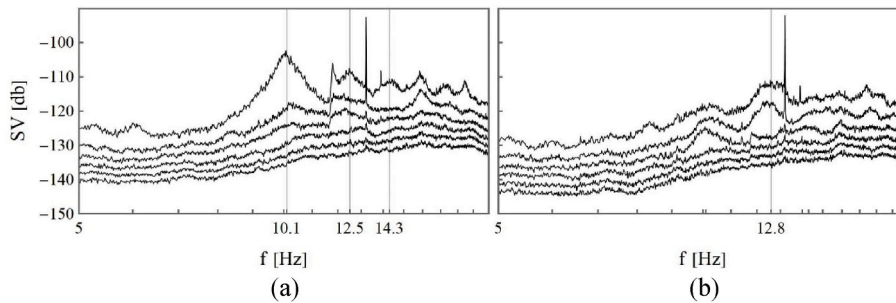


Fig. 8. Singular value (SV) spectra: (a) transversal mode shapes; (b) longitudinal mode shape. The building natural frequencies obtained by peak picking are indicated by the vertical lines.

[9] considering the factors  $\varphi$  and  $\psi_2$  for the live load. The coefficient  $\varphi = 0.8$  is fixed for the first floor and  $\varphi = 1$  for the second floor and roof, depending on the floor occupancy. The coefficient  $\psi_2 = 0.3$  is taken for the first floor and  $\psi_2 = 0.8$  for the second floor and roof, depending on

the building intended use.

The pushover curves for the 24 analyses are presented in Fig. 10, in which a thick red point represents the first significant yield. For each analysis, the over-strength ratio (OSR) is calculated as the ratio between

**Table 6**  
Comparison of numerical (NMA) and operational (OMA) modal analysis: natural frequencies, error in the estimation of natural frequencies considering the OMA as a reference and modal assurance criterion (MAC).

	Mode 1	Mode 2	Mode 3	Mode 4
NMA: frequency (Hz)	9.9	12.5	13.3	13.8
OMA: frequency (Hz)	10.1	12.5	12.8	14.3
Error (%)	2	<1	4	3
MAC (%)	90.5	70.6	62.9	29.2

$f_y$  (the plateau in the corresponding bilinear curve) and  $f_{y1}$  (the base shear associated with the thick point in Fig. 10). The behavior factor  $q$  is defined as the product of the force reduction factor  $q_0$  and the over-strength ratio  $OSR$ .

The overall resistance of this building is not significantly affected by the accidental eccentricity. In fact, in particular for the uniform load distribution, the results obtained for the three accidental eccentricity levels (0,  $\pm 5\%$ ) are similar.

The response of the building is affected by the loading direction ( $\pm$ ), in both strength and ductility. In fact, the direction of load leads to a variation in axial load and a consequent change in the dominant failure

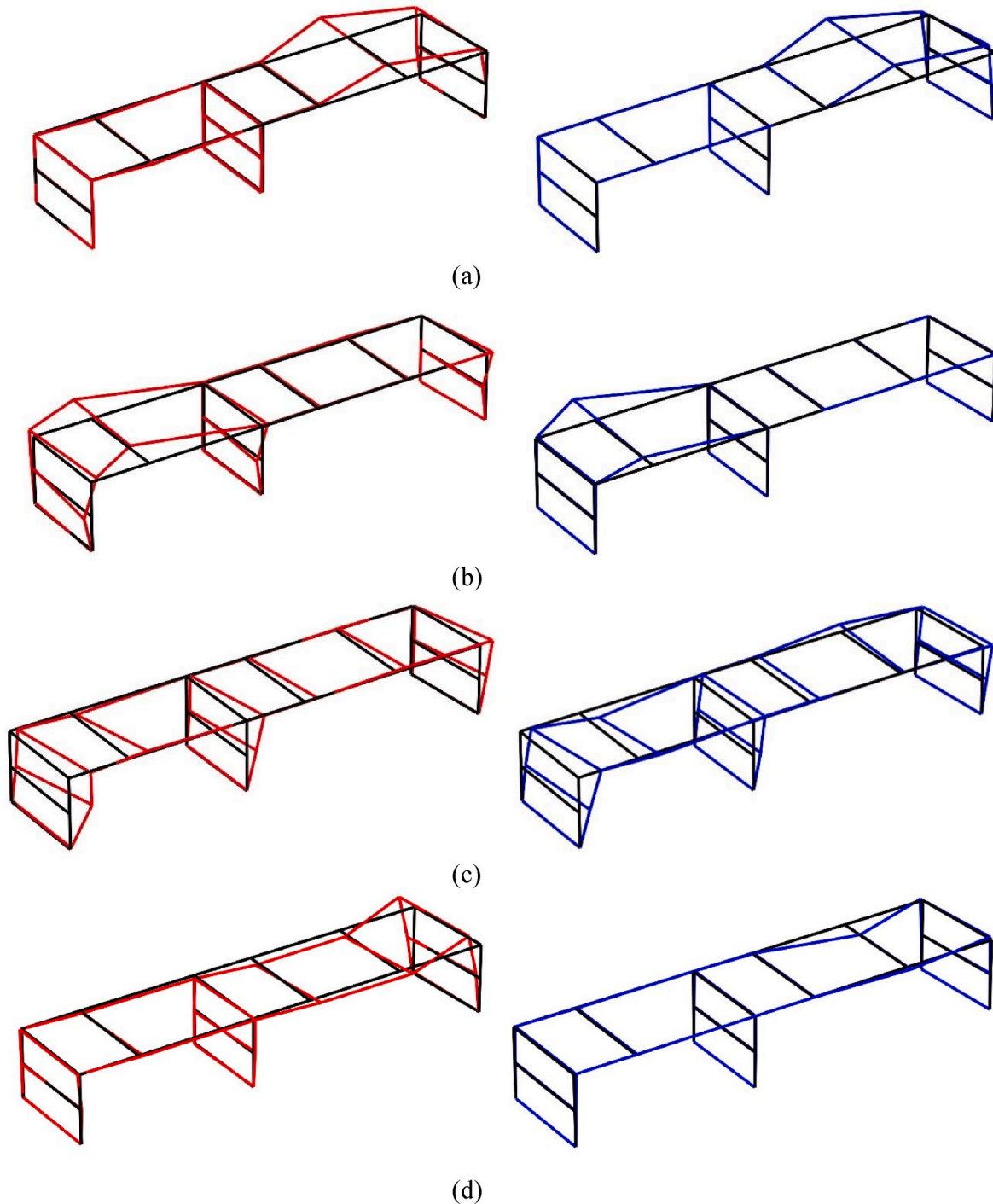


**Fig. 9.** Three-dimensional representation of the (a) first, (b) second, (c) third, and (d) four mode shapes of the analyzed CEB masonry building, obtained by operational (left) and numerical (right) modal analysis.

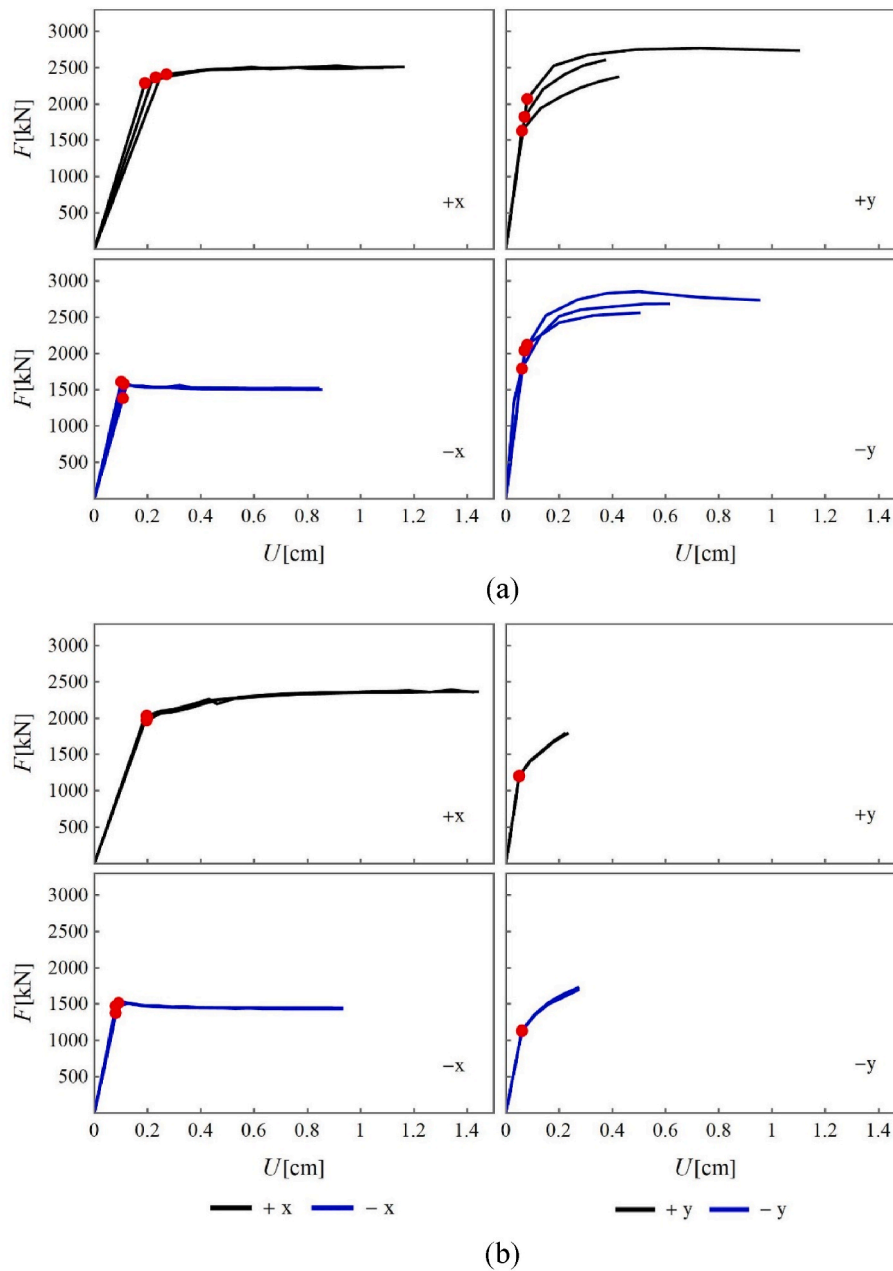


**Fig. 10.** Pushover curves for (a) uniform and (b) multimodal load distribution, obtained for load directions  $\pm x$  (left) and  $\pm y$  (right), and for three accidental eccentricity levels (0,  $\pm 5\%$ ). The first significant yield point is highlighted in each pushover curve by a circle.

mode occurring in each panel [15], affecting the location of the first pier failing and the consequent building failure. Comparing the ductility for both load directions, the ductility in the transversal  $y$ -direction is less than in the longitudinal  $x$ -direction, for the multimodal load distribution. This difference is less evident for the uniform load distribution.

#### 4.2. Force reduction factor and stability verification

The force reduction factor  $q_0$  estimated from the 24 capacity curves is presented in Tables 7–8. The fundamental period  $T_0$ , mass  $m_0$  and participation factor  $\Gamma$  of the equivalent SDOF system, as well as the yield base shear  $f_y$ , ductility capacity  $\mu_0$  and overstrength ratio  $OSR$  obtained from its capacity curve, are listed for each load combination. The minimum behavior factor  $q$  for the set of 6 load combinations, in each load direction, is indicated in bold type character. The minimum behavior factors are observed for the  $x$ -direction of loading ( $q = 2.4$ ) in the case of

uniform load distribution (Table 7) and for the  $y$ -direction ( $q = 2.1$ ) in the case of multimodal distribution (Table 8). The force reduction and behavior factor for a CEB masonry building are an original result of this research. Additional studies are necessary to confirm a convenient range of values for this construction typology.

The displacement demand  $U_t$  (performance point) of the CEB masonry building is estimated using Eq. (1), where the estimated damping ratio is  $\zeta = 2\%$  for the CEB masonry building (Section 3.1). Moreover, according to French provisions [53], the response spectrum parameters are the design ground acceleration  $a_g = 1.6 \text{ m/s}^2$  (seismic zone 4 and importance class II), soil factor  $S = 1.35$  (ground type B), and corner periods  $T_B = 0.05 \text{ s}$ ,  $T_C = 0.25 \text{ s}$  and  $T_D = 2.5 \text{ s}$ . In Tables 9–10, the displacement demand  $U_t$  (performance point) of the CEB masonry building is compared with the ultimate displacement  $U_u$  for the 24 analyses. The building capacity  $U_u$  surpasses the seismic demand  $U_t$  by a factor at least equal to 2.2 in all cases.

**Table 7**  
Behavior factor for the CEB masonry building (uniform load distribution).

Load distribution	Load combination	$T_0$ [s]	$m_0$ [kg]	$\Gamma$	$f_y$ [daN]	$\mu_0$	OSR	$q_0$	$q$
Uniform	+x	0.1403	535253	1.09	227789	4.8	1.1	2.6	2.7
Uniform	+x + e	0.1324	535253	1.09	227158	5.6	1.1	2.7	2.9
Uniform	+x-e	0.1484	535253	1.09	227729	4.2	1.0	2.4	2.4
Uniform	-x	0.1212	535253	1.09	139336	8.0	1.0	3.3	3.3
Uniform	-x + e	0.1145	535253	1.09	140382	8.8	1.0	3.4	3.4
Uniform	-x-e	0.1276	535253	1.09	140147	7.0	1.1	3.1	3.3
Uniform	+y	0.0785	406589	0.76	311206	4.1	1.3	1.9	2.5
Uniform	+y + e	0.0787	406589	0.76	354119	10.6	1.3	3.3	4.2
Uniform	+y-e	0.0805	406589	0.76	283177	4.8	1.3	2.1	2.8
Uniform	-y	0.0742	406589	0.76	360031	10.1	1.3	3.1	4.1
Uniform	-y + e	0.0728	406589	0.76	324766	6.1	1.2	2.4	2.8
Uniform	-y-e	0.0792	406589	0.76	339270	6.1	1.4	2.4	3.4

$T_0$  fundamental period,  $m_0$  mass,  $\Gamma$  participation factor,  $f_y$  yield base shear,  $\mu_0$  ductility capacity, OSR overstrength ratio,  $q_0$  force reduction factor,  $q$  behavior factor.

**Table 8**  
Behavior factor for the CEB masonry building (multimodal load distribution).

Load distribution	Load combination	$T_0$ [s]	$m_0$ [kg]	$\Gamma$	$f_y$ [daN]	$\mu_0$	OSR	$q_0$	$q$
Multimodal	+x	0.1416	535253	1.09	210561	6.6	1.1	3.1	3.6
Multimodal	+x + e	0.1432	535253	1.09	211075	6.4	1.2	3.1	3.6
Multimodal	+x-e	0.1407	535253	1.09	210843	6.3	1.1	3.0	3.4
Multimodal	-x	0.1120	535253	1.09	133711	10.7	1.0	3.7	3.7
Multimodal	-x + e	0.1071	535253	1.09	132956	11.8	1.0	3.9	3.9
Multimodal	-x-e	0.1108	535253	1.09	134183	10.5	1.0	3.7	3.7
Multimodal	+y	0.0870	406589	0.76	209454	2.9	1.3	1.6	2.1
Multimodal	+y + e	0.0877	406589	0.76	210858	3.0	1.3	1.6	2.1
Multimodal	+y-e	0.0863	406589	0.76	209691	3.0	1.3	1.6	2.1
Multimodal	-y	0.1000	406589	0.76	205194	2.8	1.4	1.6	2.2
Multimodal	-y + e	0.0992	406589	0.76	202111	2.9	1.4	1.6	2.2
Multimodal	-y-e	0.1002	406589	0.76	207582	2.7	1.4	1.5	2.1

$T_0$  fundamental period,  $m_0$  mass,  $\Gamma$  participation factor,  $f_y$  yield base shear,  $\mu_0$  ductility capacity, OSR overstrength ratio,  $q_0$  force reduction factor,  $q$  behavior factor.

**Table 9**  
Building capacity and seismic demand at the near collapse limit state (uniform load distribution).

Load distribution	Load combination	$U_t$ [cm]	$U_u$ [cm]	$U_u/U_t$	$q_u$	$q_0$
Uniform	+x	0.34	1.12	3.34	1.27	2.6
Uniform	+x + e	0.32	1.16	3.68	1.27	2.7
Uniform	+x-e	0.37	1.08	2.91	1.27	2.4
Uniform	-x	0.34	0.85	2.52	2.07	3.3
Uniform	-x + e	0.31	0.84	2.74	2.05	3.4
Uniform	-x-e	0.37	0.81	2.21	2.06	3.1
Uniform	+y	0.07	0.37	5.46	0.69	1.9
Uniform	+y + e	0.06	1.10	17.23	0.62	3.3
Uniform	+y-e	0.08	0.42	5.54	0.76	2.1
Uniform	-y	0.06	0.94	17.11	0.61	3.1
Uniform	-y + e	0.05	0.50	9.31	0.67	2.4
Uniform	-y-e	0.07	0.61	9.25	0.65	2.4

$U_t$  target displacement,  $U_u$  ultimate displacement,  $q_u$  load ratio,  $q_0$  force reduction factor.

**5. Effects of the timber slab stiffness**

Even if the seismic performance of the building is verified in terms of displacement and load capacity (Tables 9–10), the modal analysis shows the partial movement of the building in the first translational mode shapes (Fig. 9) and different inertia in the two orthogonal directions (gap in the first natural frequency for each direction, in Table 6). The lack of a dominant translational mode in  $y$ -direction, as deduced by the scattered effective mass associated with the mode shapes (Table 11), is a

**Table 10**  
Building capacity and seismic demand at the near collapse limit state (multimodal load distribution).

Load distribution	Load combination	$U_t$ [cm]	$U_u$ [cm]	$U_u/U_t$	$q_u$	$q_0$
Multimodal	+x	0.36	1.44	3.96	1.37	3.1
Multimodal	+x + e	0.36	1.42	3.95	1.37	3.1
Multimodal	+x-e	0.36	1.36	3.76	1.37	3.0
Multimodal	-x	0.31	0.93	3.04	2.16	3.7
Multimodal	-x + e	0.30	0.93	3.05	2.17	3.9
Multimodal	-x-e	0.31	0.89	2.85	2.15	3.7
Multimodal	+y	0.09	0.22	2.37	1.00	1.6
Multimodal	+y + e	0.10	0.23	2.34	1.00	1.6
Multimodal	+y-e	0.09	0.22	2.40	1.00	1.6
Multimodal	-y	0.12	0.27	2.33	1.07	1.6
Multimodal	-y + e	0.12	0.27	2.34	1.08	1.6
Multimodal	-y-e	0.11	0.27	2.36	1.06	1.5

$U_t$  target displacement,  $U_u$  ultimate displacement,  $q_u$  load ratio,  $q_0$  force reduction factor.

consequence of the high aspect ratio (almost four) and timber slab flexibility. Therefore, the impact of the in-plane stiffness of timber slab on the dynamic response of this pilot CEB masonry building is investigated.

In this research, two levels of diaphragm flexibility are compared: (a) the one-way timber floor (1W-TF) used in this pilot project (Fig. 6), and (b) a two-way reinforced timber floor (2W-RTF). The elastic mechanical parameters of the timber slab (1W-TF) are discussed in Sections 2.3 and 3.1. In the case of 2W-RTF, a 5 cm thick reinforced concrete topping is



**Table 11**  
Dynamic properties for different timber floor stiffness: one-way timber floor (1W-TF) and two-way reinforced timber floor (2W-RTF).

Mode	1W-TF				2W-RTF			
	T (s)	f (Hz)	$m_x$ (%)	$m_y$ (%)	T (s)	f (Hz)	$m_x$ (%)	$m_y$ (%)
1	0.1014	9.9	0	16	0.0685	14.6	83	0
2	0.0800	12.5	3	7	0.0645	15.5	4	28
3	0.0751	13.3	57	0	0.0425	23.5	1	46
4	0.0724	13.8	4	0	0.0397	25.2	1	1
5	0.0588	17.0	6	1	0.0379	26.4	0	5
6	0.0563	17.8	0	7	0.0319	31.3	3	0
7	0.0532	18.8	0	7	0.0285	35.1	4	0

T: natural period; f: frequency;  $m_x$ ,  $m_y$ : effective mass in x- and y-direction.

added to increase the stiffness. The concrete class is C25/30 according to Eurocode 2 (EC2, [54]). The shear modulus  $G_{12}$  and the elastic modulus in compression  $E_2$  in the secondary orthotropy direction are imposed equal to the elastic moduli of concrete  $G_c$  and  $E_c$ , respectively. In the main orthotropy direction, the equivalent elastic modulus in compression  $E_1$  is determined by considering the presence of timber joists and reinforced planking as  $(E_w A_j) / (i t_{eff}) + E_c$ , where  $E_w$  is the elastic modulus of the wood,  $E_c$  is the elastic modulus of the concrete,  $A_j$  is the joist cross-sectional area,  $i$  is the joist spacing and  $t_{eff}$  is the effective thickness of the diaphragm.

5.1. Modal analysis

The numerical modal analysis using the 3D EF model in Fig. 7 provides the results listed in Table 11, for the two timber slab

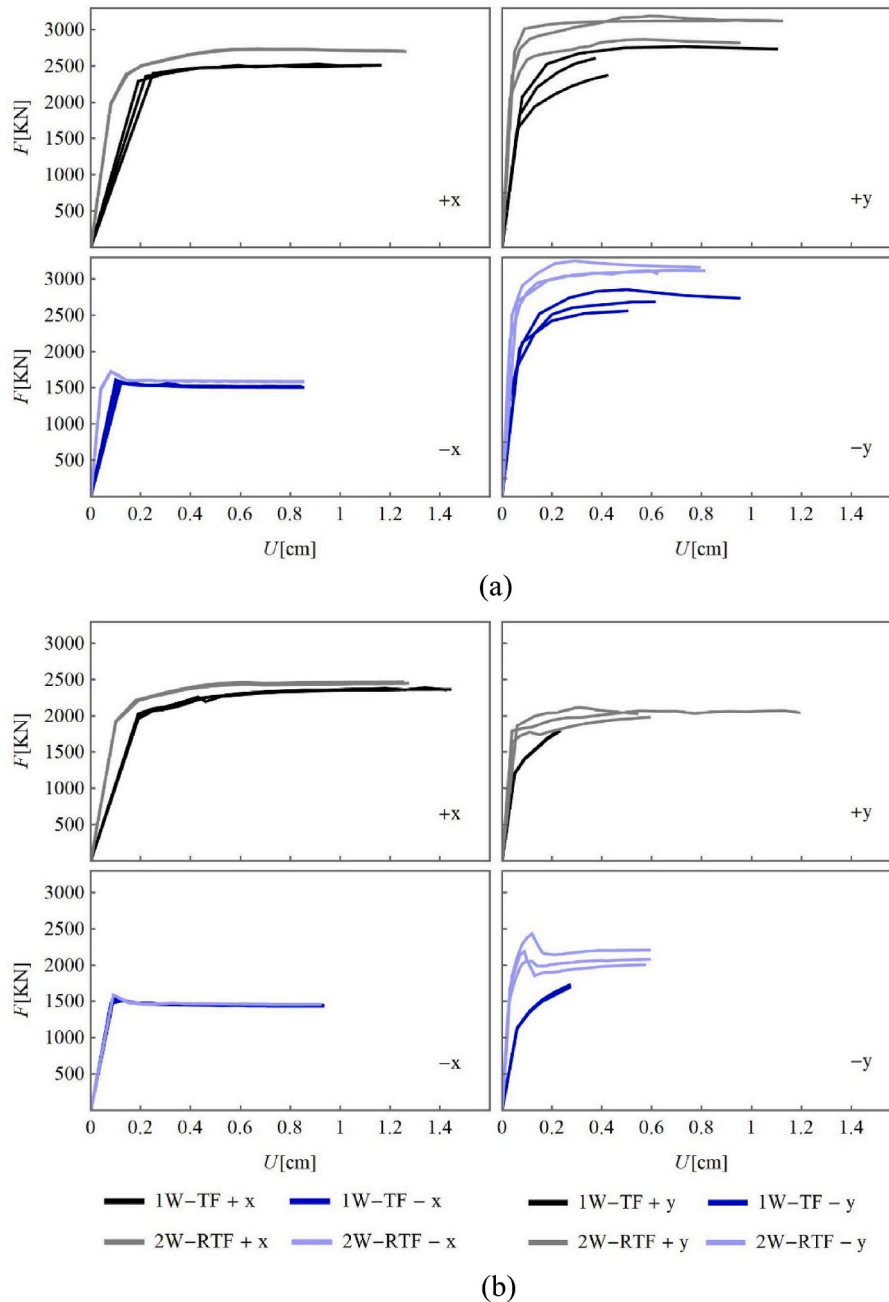


**Fig. 11.** Pushover curves for (a) uniform and (b) multimodal load distribution, obtained for load directions  $\pm x$  and  $\pm y$ , and for different timber floor stiffness: (1W-TF) one-way timber floor; (2W-RTF) two-way reinforced timber floor.

configurations. As expected, the natural frequencies increase with the diaphragm stiffness. In addition, the effective mass is much more scattered in multiple non-dominant translational modes for the 1W-TF configuration. Whereas, increasing the diaphragm stiffness leads to a concentration of the effective mass in the first translational modes (83 % for x-direction; 28 % and 46 % for y-direction). In fact, the effective mass related to the first translational modes increases with the diaphragm stiffness.

In this CEB building having a high length to width ratio, the use of a 5 cm thick concrete topping in the timber slab provides enough coupling to obtain a dominant translational mode shape in the longitudinal x-direction and to concentrate the effective mass in two translational mode shapes in the transversal y-direction (see coordinate system in Fig. 5).

### 5.2. Ductility capacity

The pushover curves obtained, for the same load combinations and distributions discussed in Section 4, are presented in Fig. 11 for the two timber floor configurations. The elastic stiffness of the structure (initial slope of the pushover curve) increases with the diaphragm stiffness, as well as the building strength and ductility for most of the load combinations. In particular, the strength and ductility increase is more evident in the weakest building direction (transversal y-direction). The ultimate to target displacement ratio increases with the timber floor stiffness for almost all the load combinations or at least it remains at the same level (Table 12).

The color map of damage level in the pilot CEB masonry building at the ultimate displacement is presented in Fig. 12, in the case of uniform load distribution in + x-direction. Comparing the damage level in the vertical structural elements of the building, the structure with the stiffer timber floor (2W-RTF in Fig. 12b) achieves a more uniform distribution of forces among the wall elements in both directions, involving also walls orthogonal to the loading direction. This redistribution of forces among the vertical wall elements, associated with the increasing stiffness of timber slabs, is coherent with the results discussed by Salvaggio et al. [21] and Zarzour et al. [23]. This suggests that a timber slab reinforced by a stiffer topping represents a good technology for masonry buildings in seismic zones, compensating for some effects of the irregularity in plan. The in-plane stiffness of the timber slab can be increased by a reinforced concrete topping or also by steel connectors.

**Table 12**  
Building ductility in the case of uniform and multimodal load distribution, for different timber floor stiffness.

Load combination	Uniform load distribution			Multimodal load distribution		
	1W-TF $\mu_0$	2W-RTF $\mu_0$	DR	1W-TF $\mu_0$	2W-RTF $\mu_0$	DR
+x	4.8	11.6	2.4	6.6	10.0	1.5
+x + e	5.6	11.5	2.0	6.4	10.0	1.6
+x - e	4.2	11.8	2.8	6.3	10.2	1.6
-x	8.0	19.7	2.4	10.7	11.0	1.0
-x + e	8.8	19.5	2.2	11.8	11.0	0.9
-x - e	7.0	19.9	2.9	10.5	11.0	1.1
+y	4.1	20.5	5.0	2.9	26.5	9.0
+y + e	10.6	19.5	1.8	3.0	8.2	2.7
+y - e	4.8	23.4	4.8	3.0	12.9	4.3
-y	10.1	15.7	1.6	2.8	16.0	5.7
-y + e	6.1	11.9	1.9	2.9	12.9	4.5
-y - e	6.1	13.6	2.2	2.7	14.8	5.4

1W-TF: one-way timber floor; 2W-RTF: two-way reinforced timber floor;  $\mu_0$ : building ductility; DR: 2W-RTF to 1W-TF ductility ratio.

## 6. Conclusion

Compressed earth block (CEB) fabrication in construction sites where fine-grained soil is present allows the reuse of local soil, removed during earthworks, and reduces energy consumption related to its collection, transport, recovery, and disposal. In this context, CEB masonry allows a low-carbon construction technology for low-rise buildings. This paper discusses the methodology developed for the seismic design of a pilot project of CEB masonry building, in a medium-high seismic hazard zone in Southern France. After the mechanical characterization of construction materials using standardized laboratory tests, the building dynamic properties (natural frequencies, mode shapes, and ductility capacity) are estimated numerically according to the equivalent frame model, with macro-elements representing the wall panels. Considering the regularity of masonry, the mechanical parameters of CEB masonry are obtained using the homogenization relationships proposed by the European building code. Then, the seismic performance is verified. In particular, the estimation of the force reduction factor, as well as the stability verification in terms of load capacity, are performed using a procedure developed by the authors. The numerical procedure was previously tested for an existing building and, in this research, it is applied for the first time for the seismic design of a new CEB masonry building. The force reduction and behavior factor for a CEB masonry building are an original result of this research. The obtained values represent a reference for further CEB masonry buildings, even if additional studies are necessary to confirm a convenient range of values for this construction typology.

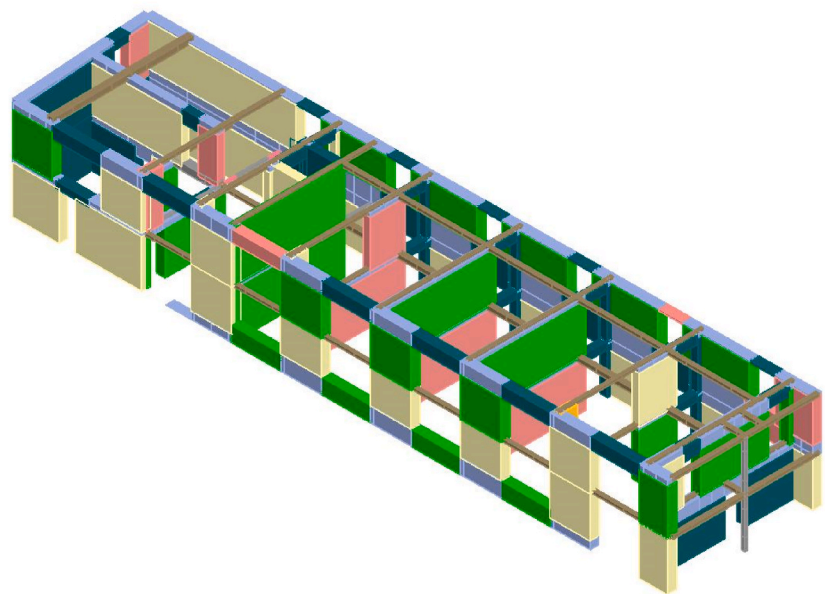
The structural response to ambient vibration is recorded during a measurement campaign so that the three-dimensional building model is validated by comparing the dynamic features obtained through numerical and operational modal analysis (natural frequencies and mode shapes). This model validation methodology highlights the impact of timber slab stiffness on the dynamic response of the CEB masonry building. After calibration of the timber slab stiffness, negligible discrepancies are obtained for the first four natural frequencies, and the mode shapes are accurately reproduced. Consequently, the elastic mechanical parameters of CEB masonry and plum concrete are validated.

The analysis of mode shapes and effective masses suggests the improvement of the building conception to obtain global mode shapes with effective masses concentrated in few mode shapes, inducing a better dynamic behavior of the CEB masonry building. Increasing the diaphragm stiffness (maintaining the same wall configuration) improves the building ductility and load-bearing capacity. In particular, a timber floor reinforced by a stiffer topping provides sufficient wall coupling, compensating plan irregularities.

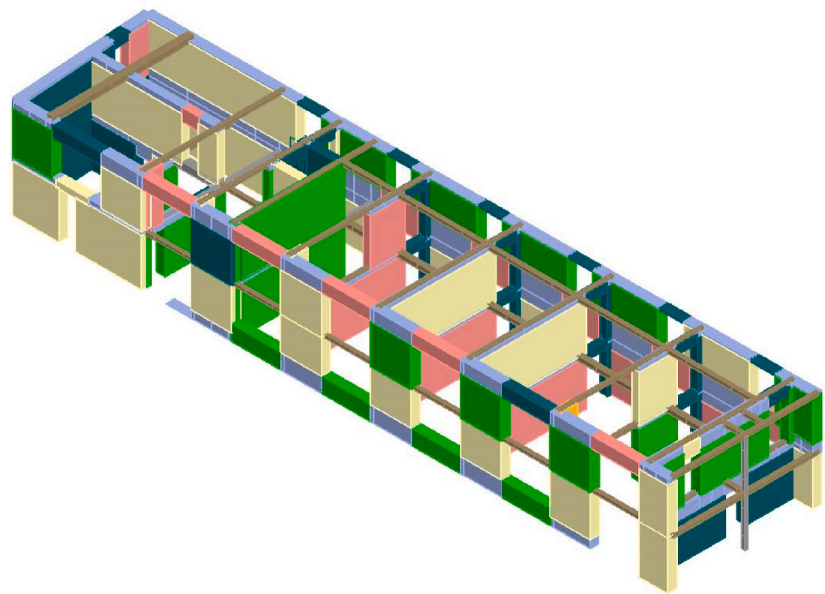
The adopted model validation methodology, using the structural response to ambient motion, allows the corroboration of elastic properties. Further research is foreseen to perform experimental cyclic pushover tests on wall scale specimens to get more accurate results concerning the masonry plastic behavior, in particular in terms of ductility, friction angle, and drift capacity of piers.

## Data and resources

In this research, the 3D masonry building model is developed using 3Muri software by S.T.A DATA (Release 13.9.0.1). The measurement campaign for the modal identification of the building is performed by the Repsody team of CEREMA. The experimental results of laboratory tests on materials (compression tests on compressed earth block specimens, shear tests on block-mortar interface, and compression and shear tests on plum concrete cylindrical specimens) provided by FILIATER company, are carried out by the Laboratoire de Génie Civil et Bâtiment (LGCB/LTDS) of the École Nationale des Travaux Publics de l'État (ENTPE) in Lyon (France).



(a) 1W-TF  
 $F=2509 \text{ KN}$ ,  $U_u=1.12 \text{ cm}$



<span style="color: green;">■</span> Undamaged	<span style="color: yellow;">■</span> Shear damage	<span style="color: orange;">■</span> Incipient shear failure
<span style="color: red;">■</span> Bending damage	<span style="color: blue;">■</span> Uncompressed	

(b) 2W-RTF  
 $F=2707 \text{ KN}$ ,  $U_u=1.25 \text{ cm}$

**Fig. 12.** Colormap of the damage level in the geo-sourced element for uniform load distribution and load direction + x, at the ultimate displacement: (a) one-way timber floor; (b) two-way reinforced timber floor. The attained base shear force  $F$  and ultimate displacement  $U_u$  are indicated.

**CRedit authorship contribution statement**

**Noura Zarzour:** Data curation, Formal analysis, Investigation, Software, Validation, Writing – original draft, Writing – review & editing. **Maria Paola Santisi d’Avila:** Conceptualization, Formal analysis, Investigation, Methodology, Project administration, Supervision, Writing – original draft, Writing – review & editing. **E. Diego Mercerat:** Data curation, Investigation, Validation. **Luca Lenti:** Supervision,

Writing – review & editing. **Michel Oggero:** Data curation, Funding acquisition, Supervision.

**Declaration of competing interest**

The authors declare that they have no known competing financial interests or personal relationships that could have appeared to influence the work reported in this paper.

## Data availability

Data will be made available on request.

## Acknowledgments

This research is carried out in the framework of the French National Project “Mechanical behavior of compressed earth blocks for sustainable building construction in seismic areas” (DYNATERRE, ANR-23-CE04-0015-01) funded by the French National Research Agency. This work has been funded by the region SUD (South-Eastern France) and by FILIATER company through a doctoral fellowship.

## References

- [1] Prikryl R, Török Á, Theodoridou M, Gomez-Heras M, Miskovsky K. Geomaterials in construction and their sustainability: understanding their role in modern society. *Geol Soc Spec Publ* 2016;416(1):1–22.
- [2] Turco C, de Paula Junior Campos A, Teixeira RE, Mateus R. Optimisation of Compressed Earth Blocks (CEBs) using natural origin materials: a systematic literature review. *Construct Build Mater* 2021;309:125140.
- [3] Valenzuela M, Ciudad G, Cárdenas JP, Medina C, Salas A, Oñate A, Pincheira G, Attia S, Tuninetti V. Towards the development of performance-efficient compressed earth blocks from industrial and agro-industrial by-products. *Renew Sustain Energy Rev* 2024;194:114323.
- [4] Bahar R, Benazzoug M, Kenai S. Performance of compacted cement stabilized soil. *Cem Concr Compos* 2004;26(7):811–20.
- [5] Mahdad M, Benidir A. Hydro-mechanical properties and durability of earth blocks: influence of different stabilisers and compaction levels. *Int. J. Sustain. Build. Technol. Urban. Dev.* 2018;9:44–60.
- [6] Sitton JD, Zeinali Y, Heidarian WH, Story BA. Effect of mix design on compressed earth block strength. *Construct Build Mater* 2018;158:124–31.
- [7] Teixeira ER, Machado G, De Adilson P, Guarnier C, Fernandes J, Silva SM, Mateus R. Mechanical and thermal performance characterisation of compressed earth blocks. *Energies* 2020;13(11):2978.
- [8] Miranda E, Bertero VVB. Evaluation of strength reduction factors for earthquake-resistant design. *Earthq Spectra* 1994;10(2):357–79.
- [9] EN 1998-1. Eurocode 8: design of Structures for earthquake resistance - Part 1: general rules, seismic actions and rules for buildings. Brussels, Belgium: CEN; 2004.
- [10] FEMA P695. Quantification of building seismic performance factors. Washington DC, USA: US Department of Homeland Security, FEMA; 2009.
- [11] Chopra AK. Dynamics of structures: theory and applications to earthquake engineering. Upper Saddle River, New Jersey: Prentice-Hall; 2001.
- [12] Priestley MNJ, Calvi GM, Kowalski M. Displacement-based seismic design of structures. Pavia, Italy: IUSS Press; 2007.
- [13] Magenes G, Della Fontana A. Simplified non-linear seismic analysis of masonry buildings. Proceedings of the 5th international masonry conference 1998;8:190–5.
- [14] Belmouden Y, Lestuzzi P. An equivalent frame model for seismic analysis of masonry and reinforced concrete buildings. *Construct Build Mater* 2009;23:40–53.
- [15] Lagomarsino S, Penna A, Galasco A, Cattari S. TREMURI program: an equivalent frame model for the nonlinear seismic analysis of masonry buildings. *Eng Struct* 2013;56:1787–99.
- [16] Penna A, Lagomarsino S, Galasco A. A nonlinear macroelement model for the seismic analysis of masonry buildings. *Earthq Eng Struct Dynam* 2014;43(2): 159–79.
- [17] Galasco A, Lagomarsino S, Penna A. On the use of pushover analysis for existing masonry buildings. Proc. 1st European Conf. Earthquake Eng. Seismol. 2006 Geneva, Switzerland, Paper No. 1080.
- [18] Magenes G, Calvi GM. In-plane seismic response of brick masonry walls. *Earthq Eng Struct Dynam* 1997;26:1091–112.
- [19] Calderini C, Cattari S, Lagomarsino S. In-plane strength of unreinforced masonry piers. *Earthq Eng Struct Dynam* 2009;38(2):243–67.
- [20] Beyer K, Mangalathu S. Review of strength models for masonry spandrels. *Bull Earthq Eng* 2013;11:521–42.
- [21] Salvalaggio M, Sbrogiò L, Pavanetto M, Valluzzi MR. Evaluation of the effect of compatible interventions applied to horizontal components of URM buildings with EFM and FEM models. The case of palazzo Carraro in Noale (Italy). Proceedings of the 7th international conference on computational methods in structural dynamics and earthquake engineering. Greece: Crete; 2019.
- [22] Pavanetto M, Sbrogiò L, Salvalaggio M, Valluzzi MR. Equivalent frame modelling of an unreinforced masonry building in finite element environment. Proc. XXIV AIMETA Conf. 2019 2020. Rome, Italy.
- [23] Zarzour N, Santisi d’Avila MP, Lenti L, Oggero M. Impact of in-plane stiffness of floors on the seismic response of geo-sourced masonry. Proc. 18th World Conf. Earthquake Eng. 2024 Milan, Italy.
- [24] Environmental code (Code de l’environnement). Prévention du risque sismique, Article D563-8-1, Partie réglementaire, Livre V, Titre VI, Chapitre III, Section 1, Sous-section 1, Paris, France. 2023 (in French).
- [25] Diaferio M, Foti D, Giannoccaro NI, Ivorra S. Optimal model through identified frequencies of a masonry building structure with wooden floors. *Int. J. Mech.* 2014; 8:282–8.
- [26] Fernandez Lorenzo GW, Santisi d’Avila MP, Deschamps A, Bertrand E, Mercerat ED, Foundotos L, Courboulex F. Numerical and empirical simulation of linear elastic seismic response of a building: the case of Nice Prefecture. *Earth Spectra* 2018;34:169–96.
- [27] Capanna I, Cirella R, Aloisio A, Di Fabio F, Fragiaco M. Operational modal analysis and non-linear dynamic simulations of a prototype low-rise masonry building. *Buildings* 2021;11(10):1–22. 471.
- [28] Brincker R, Zhang L, Andersen P. Modal identification of output-only systems using frequency domain decomposition. *Smart Mater Struct* 2001;10(3):441–5.
- [29] Brincker R, Ventura C. Introduction to operational modal analysis. United Kingdom: Wiley; 2015.
- [30] Krawinkler H, Seneviratna GDPK. Pros and cons of a pushover analysis of seismic performance evaluation. *Eng Struct* 1998;20(4–6):452–64.
- [31] EN 1998-3. Eurocode 8: design of Structures for earthquake resistance - Part 3: assessment and retrofitting of buildings. Brussels, Belgium: CEN; 2005.
- [32] Fajfar P. A nonlinear analysis method for performance-based seismic design. *Earthq Spectra* 2000;16(3):573–92.
- [33] Zarzour N, Santisi d’Avila MP, Mercerat ED, Lenti L, Oggero M. Behavior factor estimation for seismic design of unreinforced masonry buildings. *Case Stud Constr Mater* 2023;19:e02483.
- [34] NF P94-068. Soils : investigation and testing. Measuring of the methylene blue adsorption capacity of a rocky soil. Determination of the methylene blue of a soil by means of the stain test. Afnor, Paris, France 1998.
- [35] NF P94-057. Soils investigation and testing. Granulomet Anal. Hydrometer Meth 1992. Afnor, Paris, France.
- [36] NF P11-300. Earthworks. Classification of materials for use in the construction of embankments and capping layers of road infrastructures. Paris, France: Afnor; 1992.
- [37] NF EN 197-1. Cement - Part 1: composition, specifications and conformity criteria for common cements. Paris, France: Afnor; 2012.
- [38] NF EN 206. Concrete: specification, performance, production and conformity. 2014. Afnor, Paris, France.
- [39] NF EN 772-1. Methods of test for masonry units - Part 1 : determination of compressive strength. Paris, France: Afnor; 2001.
- [40] NF EN 12390-3. Testing hardened concrete - Part 3 : compressive strength of test specimens. Afnor 2003. Paris, France.
- [41] NF EN 12390-6. Testing hardened concrete - Part 6 : tensile splitting strength of test specimens. 2012. Afnor, Paris, France.
- [42] EN 1996-1-1. Eurocode 6- Design of masonry structures - Part 1-1: general rules for reinforced and unreinforced masonry structures. Brussels, Belgium: CEN; 2005.
- [43] Binda L, Gambarotta L, Lagomarsino S, Modena C. A multilevel approach to the damage assessment and seismic improvement of masonry buildings in Italy. In: Bernardini A, editor. Seismic damage to masonry buildings. first ed. London, UK: Taylor & Francis group; 1999. p. 170–95.
- [44] NF EN 1194. Timber structures - glued laminated timber - strength classes and determination of characteristic values. Paris, France: Afnor; 1999.
- [45] NF EN 12369-1. Wood based panels - characteristic values for structural design - Part 1: OSB, particleboards and fibreboards. Paris, France: Afnor; 2001.
- [46] Beyer K, Tondelli M, Vanin F, Petry S, Paparo A. Seismic behaviour of unreinforced masonry buildings with reinforced concrete slabs: assessment of in-plane and out-of-plane response. Rep. Swiss Federal Off. Environ. 2015.
- [47] Al Aqtash U, Bandini P. Influence of wall thickness and water content on the out-of-plane stability of adobe walls. *Infrastructures* 2020;5(9):78.
- [48] Michel C, Guéguen P, Bard PY. Dynamic parameters of structures extracted from ambient vibration measurements: an aid for the seismic vulnerability assessment of existing buildings in moderate seismic hazard regions. *Soil Dynam Earthq Eng* 2008;28(8):593–604.
- [49] Pastor M, Binda M, Harčarik T. Modal assurance criterion. *Procedia Eng* 2012;48: 543–8.
- [50] Tomažević M. Earthquake-resistant design of masonry buildings. London, U.K: Imperial College Press; 1999.
- [51] NTC2018. Decreto Ministeriale 17 Gennaio 2018: Aggiornamento delle Norme tecniche per le costruzioni (in Italian), S.O. No. 8 alla G.U. del 20 Febbraio 2018, No. 42. Rome, Italy: Ministero delle Infrastrutture e dei Trasporti; 2018.
- [52] NF EN 1991-1-1. Eurocode 1 - actions on structures - Part 1-1 : general actions - densities, self weight, imposed loads for buildings. Paris, France: Afnor; 2003.
- [53] Decree of October 22. Arrêté du 22 octobre 2010 relatif à la classification et aux règles de construction parasismique applicables aux bâtiments de la classe dite à risque normal, version en vigueur au 19 octobre 2021. Official Journal of the French Republic; 2010 (in French).
- [54] EN 1992-1-1. Eurocode 2: design of concrete structures - Part 1-1: general rules and rules for buildings. Brussels, Brussels: CEN; 2004.